ACS OMEGA

http://pubs.acs.org/journal/acsodf

Article

In Situ Scanning Transmission Electron Microscopy Study of MoS_2 Formation on Graphene with a Deep-Learning Framework

Yeongdong Lee, Jongyeong Lee, Handolsam Chung, Jaemin Kim, and Zonghoon Lee*

Cite This: *ACS Omega* 2021, 6, 21623−21630

Read Online

ACCESS | Metrics & More | Article Recommendations | Supporting Information

ABSTRACT: Atomic-scale information is essential for understanding and designing unique structures and properties of two-dimensional (2D) materials. Recent developments in in situ transmission electron microscopy (TEM) and scanning transmission electron microscopy (STEM) enable research to provide abundant insights into the growth of nanomaterials. In this study, 2D MoS_2 is synthesized on a suspended graphene substrate inside a TEM column through thermolysis of the ammonium tetrathiomolybdate $(NH_4)_2MoS_4$ precursor at 500 °C. To avoid misinterpretation of the in situ STEM images, a deep-learning framework, DeepSTEM, is developed. The DeepSTEM framework successfully reconstructs an object function in atomic-resolution STEM imaging for accurate determination of the atomic structure and dynamic analysis. In situ STEM imaging with DeepSTEM enables observation of the edge configuration, formation, and reknitting progress of MoS_2 clusters with the formation of a mirror twin boundary. The synthesized MoS_2/graphene heterostructure shows various twist angles, as revealed by atomic-resolution TEM. This deep-learning framework-assisted in situ STEM imaging provides atomic information for in-depth studies on the growth and structure of 2D materials and shows the potential use of deep-learning techniques in 2D material research.

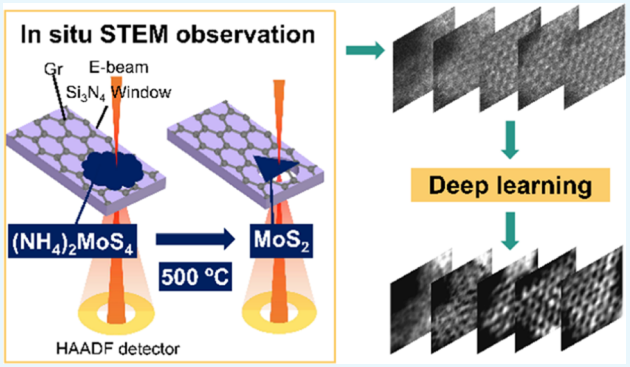

1. INTRODUCTION

In recent years, researchers have explored two-dimensional (2D) materials and their heterostructures, focusing on their layered structure and unique properties that seem promising for future applications, including field-effect transistors, diffusion barriers, liners, sensors, batteries, and optoelectronic devices.[1−5] The nanostructures of 2D materials, such as atomic defects, edge configuration, and domain size, impact their physical and chemical properties and applications. Therefore, information about the nanostructure of 2D materials is essential for understanding and designing the required properties for a dedicated application.

Transition metal dichalcogenides (TMDs) exhibit attractive properties, and molybdenum disulfide (MoS_2) is the most researched material among TMDs anticipated to use for electronics and photonics.[6] However, the low charge mobility and contact resistance with metal electrodes have limited their use.[7,8] One of the solutions is the MoS_2/graphene heterostructure. The MoS_2/graphene 2D heterostructure shows remarkable performance in electronic applications with low contact resistance with graphene as an electrode.[1,9] However, the fabrication and thermal budget of the MoS_2/graphene heterostructure also matter for their use. The transferring processes for stacking MoS_2 on graphene can adopt contamination introducing degradation of properties. The direct synthesis of MoS_2 on graphene or vice versa is required. Also, the growth temperature is important to integrate the structure in the complementary metal-oxide-semiconductor (CMOS) system with extraordinary properties.

The thermolysis-driven MoS_2 synthesis method is a promising pathway for the MoS_2/graphene heterostructure.[10] The $(NH_4)_2MoS_4$ thermally decomposes into MoS_3 at 160−270 °C, with releases of NH_3 and H_2S. Then, the MoS_2 forms at over 270 °C from MoS_3 with the release of sulfur.[11,12] Its growth temperature is compatible with CMOS technology. Recent studies have achieved layer-number control and wafer-scale growth of MoS_2 with spin coating of the $(NH_4)_2MoS_4$ precursor and heating.[13,14]

Recent progress in in situ transmission electron microscopy (TEM) and in situ scanning transmission electron microscopy-(STEM) have provided insights into the growth of 2D materials, with atomic resolution and the implementation of growth conditions of the existing methods.[15] In situ TEM/STEM is an effective tool for the manipulation of structures

Received: June 8, 2021
Accepted: August 2, 2021
Published: August 10, 2021

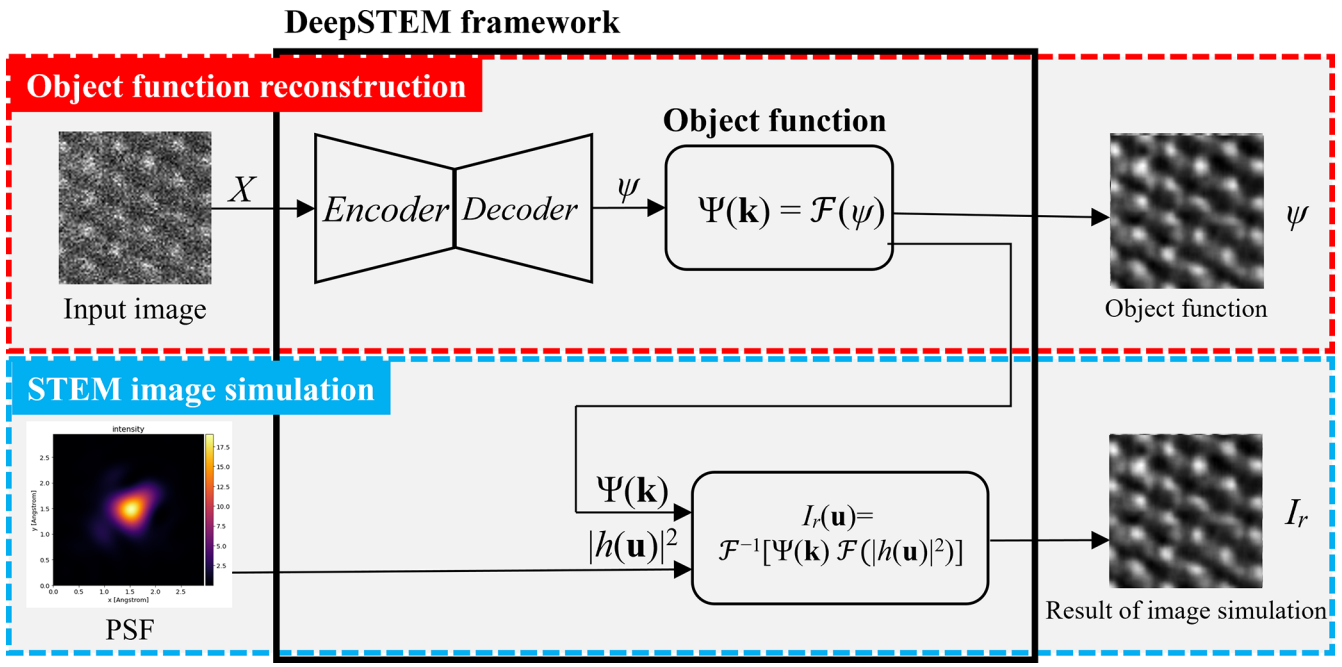

Figure 1. Structure of the DeepSTEM framework. Input images are decoded to ψ, which corresponds to the object function of the STEM image. I_r is the result of the STEM image simulation when applying the PSF to the Fourier transform of the reconstructed object function.

with an electron beam, simultaneously analyzing whether desired or novel nanostructures have been achieved.[16,17] The insights into the structure and formation are necessary for dedicated configuration synthesis of MoS_2 by thermolysis. Several studies have reported efforts devoted to understanding thermolysis-driven growth using in situ TEM/STEM.[18−20] The thermolysis of the $(NH_4)_2MoS_4$ precursor on silicon nitride leads to a vertical MoS_2 structure at 400 °C.[18] On the other hand, a horizontal MoS_2 structure was attained on a carbon film as a substrate.[19] However, an atomic-scale understanding of MoS_2 formation on graphene by thermolysis has not yet been revealed.

In situ TEM/STEM images can often be misinterpreted owing to aberrations in the optic system of TEM. Hence, in the case of in situ STEM, light elements, specimen drift, and low-dose imaging for time resolution, as well as electron beam-sensitive materials, make it difficult to understand the exact atomic structure and evolution of 2D materials. Exit-wave reconstruction and object function reconstruction have been developed to avoid this misinterpretation.[21−24] It facilitates studies of rapid movement of atoms in atomic-resolution TEM. However, the high-angle annular dark-field STEM (HAADF-STEM) analysis relies on HAADF-STEM image simulation. The result of the HAADF-STEM image simulation is compared with the experimental raw data to match the expected and detected structures, relying on human know-how. Moreover, in the case of atomic-scale dynamics study, each frame needs to be examined using simulation. The object function reconstruction using a single image for STEM imaging is necessary for atomic-scale dynamics study. The most prominent method is Wiener filtering, which is a linear denoising solution.[25] However, it divides out the contrast transfer function in the reciprocal lattice, resulting in a constant transfer function without decay.[24] The constant transfer function from the Wiener filter can introduce artifacts in the STEM image.[24] Our solution is deep-learning-based object function reconstruction from the considered factors by the probe function. Deep learning has been solving challenges in electron microscopy.[26] Recently, deep learning of the simulation data set recognized the local atomic structure in high-resolution TEM (HRTEM) images.[27] Another deep learning using experimental HRTEM data set has been developed to reconstruct the exit wave from a single image with real microscope's aberration parameters from the so-called Zemlin tableau method.[28] In this regard, a deep-learning framework in this study also shows the potential of deep learning in electron microscopy.

In this study, we investigated the formation of MoS_2 on a suspended graphene substrate inside a TEM column through thermolysis of the $(NH_4)_2MoS_4$ precursor at 500 °C with a heating holder. Atomic-resolution TEM/STEM shows the structure of the grown MoS_2 and the configuration of the MoS_2/graphene heterostructure. The dynamic structural evolution with thermal energy and electron-beam irradiation was investigated by in situ HAADF-STEM imaging. HAADF-STEM imaging can exclude a signal from the graphene substrate under incoherent conditions. In dynamics analysis, it can prevent the misinterpretation of object materials' non-periodic step structures. However, the experimental HAADF-STEM images were deteriorated by elevated temperature, specimen drift, and the low electron-dose rate for minimizing the effect of electron-beam irradiation on the structural evolution of MoS_2 on graphene. In addition, the recognition of the sulfur atoms of MoS_2, which are relatively light, was difficult with raw experimental data. We present the deep-learning framework for object function reconstruction for HAADF-STEM studies of the structure and dynamics of 2D materials. We conducted a fast Fourier transform (FFT)-based deconvolution with the deep-learning framework by including an HAADF-STEM image simulation equation with a precalculated probe function for the actual optical system conditions, which were measured as aberrations. With the assistance of the deep-learning framework, we elucidate the precise structure of MoS_2 and investigate the structural

https://doi.org/10.1021/acsomega.1c03002
ACS Omega 2021, 6, 21623−21630

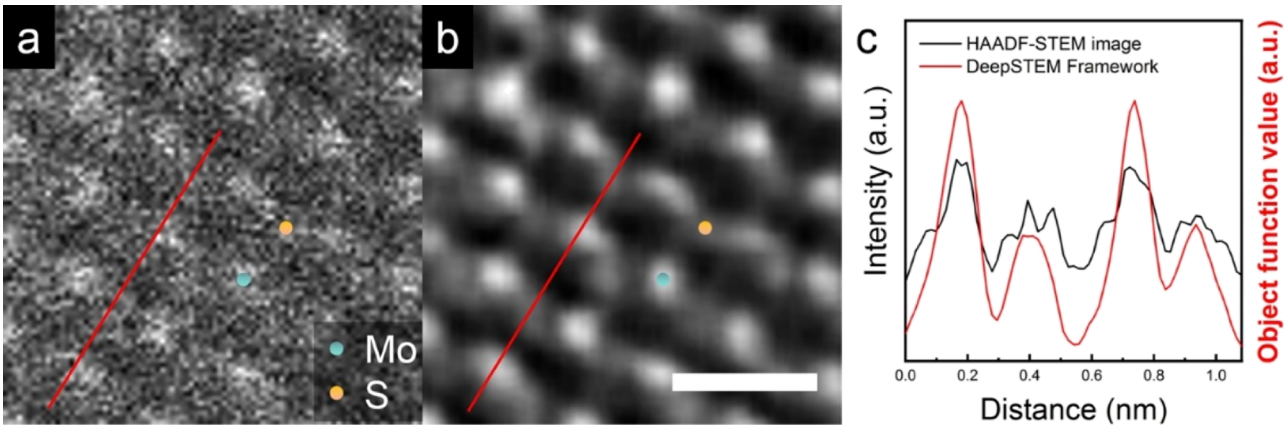

Figure 2. (a) Atomic-resolution HAADF-STEM image of MoS_2 on graphene. (b) Image of the reconstructed object function. (c) Intensity profiles of the experimental HAADF-STEM image and image of reconstructed object function are plotted as solid red lines from lower left to upper right in each image. The scale bar is 0.5 nm. Mo and S atoms are represented by cyan and orange spheres.

evolution of MoS_2 on graphene including edge configuration, formation, and reknitting progress. Atomic-resolution TEM shows a MoS_2/graphene 2D heterostructure through thermolysis, exhibiting various twist angles without a specific orientation.

2. RESULTS AND DISCUSSION

We propose a deep-learning framework called the DeepSTEM framework. HAADF-STEM imaging has been used to accurately determine the structure and observe the dynamics of the nanostructure of MoS_2 because HAADF-STEM imaging can directly identify the molybdenum and sulfur atoms with atomic number (Z)-dependence contrast, called Z contrast imaging, and an incoherent imaging feature.[29] However, the identification of the exact structure with dynamics is difficult because of the elevated temperature and specimen drift. To use in situ HAADF-STEM imaging for dynamical analysis, it is also necessary to decrease the electron-dose rate for better time resolution and minimizing the effects of electron-beam irradiation on the specimen. Hence, the relatively light sulfur atoms in MoS_2 are not discernible owing to the low intensity. To observe the sulfur atoms using in situ STEM dynamics, object function reconstruction is essential.

The DeepSTEM framework consists of two main parts: an object function reconstruction part and a STEM image simulation (Figure 1). The object function reconstruction part, denoted by the red dashed line in Figure 1, has an encoder, decoder, and input image (X), which is an HAADF-STEM image obtained from the HAADF detector, and an object function (ψ). The object function reconstruction part is a variant of the convolutional autoencoder.[30] Each encoder and decoder consists of four sequential layers, and an activation function, rectified linear unit (ReLU), was used in each layer. The output of the decoder is the object function ψ. The object function ψ is the projected structure of the specimen.[23] An activation function of the decoder is the zero-centered hyperbolic tangent. At the end of the decoder, there is a convolutional layer of 1×1 size 1 kernel without the activation function. The details of the DeepSTEM are in Supporting Information.

Then, this object function reconstruction subsystem finds the relationship between X and ψ. Ψ is defined as the FFT of ψ as follows

$$\Psi(\mathbf{k}) = \mathcal{F}\{\psi(\mathbf{u})\} \tag{1}$$

where $\mathbf{u}$ is a 2D position vector in the object plane and $\mathbf{k}$ is a 2D position vector in a reciprocal plane conjugate to $\mathbf{u}$.

In the STEM image simulation part denoted by the blue dashed line, I_r represents the STEM image simulation results acquired from applying the precalculated probe function with the object function as follows

$$I_r(\mathbf{u}) = \mathcal{F}^{-1}[\Psi(\mathbf{k})\mathcal{F}\{|h(\mathbf{u})|^2\}] \tag{2}$$

where $|h(\mathbf{u})|^2$ is the point spread function (PSF). The PSF $|h(\mathbf{u})|^2$ is precalculated with the experimental optic system conditions, aberrations being measured by the Zemlin tableau method.[31]

The DeepSTEM is a neural network that reconstructs the object function ψ as follows

$$\text{loss} = \|X(\mathbf{u}) - I_r(\mathbf{u})\|^2 \tag{3}$$

We used the ADAM optimization algorithm, an extension to stochastic gradient descent, to update parameters that minimize the loss function in the DeepSTEM framework with an initial learning rate of 2×10^{-5} and default parameters.[32]

Figure 2a shows the HAADF-STEM image of a MoS_2 monolayer grown on suspended graphene in the TEM column using an in situ heating holder. The monolayer graphene sheet was synthesized by chemical vapor deposition (CVD).[33,34] A heating chip mounted on the heating holder was perforated by a focused ion beam. Then, the monolayer graphene was transferred onto the perforated heating chip for suspended graphene (Figure S1). The $(NH_4)_2MoS_4$ precursor was dispersed in *N*,*N*-dimethylformamide (DMF) with 0.1 wt % solution and dropped onto suspended graphene on the heating chip with a micropipette. The thermolysis of the precursor for the in situ STEM growth of MoS_2 proceeded at a temperature of 500 °C. The temperature of the heating chip was elevated to 500 °C immediately (~1 s). The synthesized MoS_2 was recognized as a monolayer by Z-contrast imaging. Figure 2b shows an image of the reconstructed object function output by the DeepSTEM framework. Because MoS_2 is a monolayer, the object function corresponds to the atomic structure of the specimen with Z-contrast. The image of the reconstructed object function made it possible to distinguish between Mo and S with high contrast, as shown in Figure 2c. Comparing

https://doi.org/10.1021/acsomega.1c03002
ACS Omega 2021, 6, 21623−21630

the results obtained with the DeepSTEM framework with the experimental HAADF-STEM image, we concluded that the DeepSTEM framework reconstructed an object function that represents the projected atomic structure of the specimen (Figure 2c).

Using the DeepSTEM framework, we identified the edge configuration of in situ STEM-grown MoS_2 on suspended graphene. Hexagonal 2D materials primarily exhibit two types of edges: zigzag and armchair. Among them, in the case of MoS_2, zigzag edges are commonly predicted and observed, with the direction of $(10\bar{1}0)$ Mo-terminated zigzag (Mo-ZZ) and $(\bar{1}010)$ sulfur-terminated zigzag (S-ZZ) depending on growth conditions and chemical potential.[35−38] Because these edge structures can alter the electronic and magnetic properties of MoS_2 clusters,[39] their precise identification is necessary. The corresponding object function reconstruction of HAADF-STEM images (Figure 3a−c) enables accurate identification of

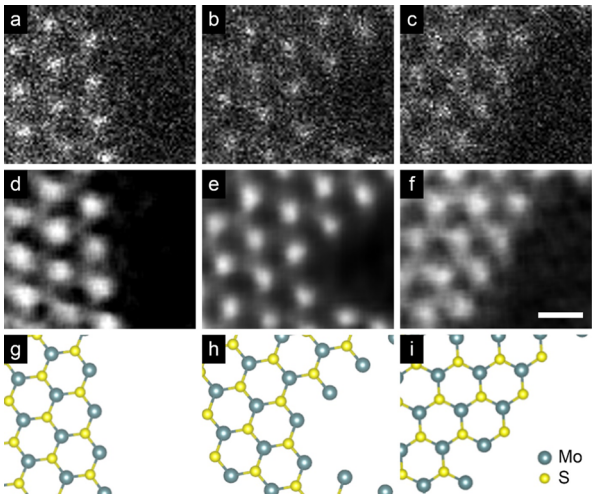

Figure 3. (a−c) Atomic-resolution HAADF-STEM images showing the edge configurations. The image was taken at a temperature of 500 °C. (d−f) Images of the reconstructed object function of (a−c) showing (d) Mo-ZZ, (e) Mo-Klein, and (f) S-ZZ. The scale bar is 0.5 nm. (g−i) Schematic atomic models based on the interpretation of (d−f). Mo and S atoms are represented by cyan and yellow spheres, respectively.

sulfur atoms, as shown in Figure 3d−f. The MoS_2 clusters predominantly have Mo-ZZ edges (Figure 3d) and Mo-Klein edges (Mo atoms bound with the S-ZZ chain, Figure 3e,f) and rarely have S-ZZ (Figure 3f). Under Mo-rich conditions, the formation energies of Mo-ZZ and Mo-Klein edges are comparable, and these edges have lower formation energies than S-ZZ edges and sulfur-attached Mo-ZZ edges.[37] Therefore, our experimental growth conditions for in situ STEM MoS_2 formation on graphene by thermolysis can be concluded to be Mo-rich.

The structural evolution of MoS_2 on graphene during formation was analyzed using in situ STEM imaging with the DeepSTEM framework. Figure 4 shows time-elapsed images of the reconstructed object function during the formation of MoS_2 on graphene while holding temperature at 500 °C. First, a MoS_x cluster is on the graphene substrate, as shown in Figure 4a. The Mo atoms do not show a periodic and ordered nanostructure. Then, the MoS_x cluster reconstructs the hexagonal lattice structure of MoS_2 with thermal energy under electron-beam irradiation, as shown in Figure 4b,c. Here, there was no merging of other MoS_x clusters. The MoS_2 cluster shows a truncated triangular shape with Mo-ZZ, Mo-Klein, and S-ZZ edges, as shown in Figure 4c. The remaining MoS_x clusters, indicated by white arrows, continue to form a MoS_2 cluster. After subsequent scans, the upside MoS_x cluster continuously transformed into a MoS_2 cluster, as shown in Figure 4d. The downside MoS_x cluster finally transformed into a MoS_2 cluster, as shown in Figure 4e. The MoS_2 cluster in Figure 4e shows a triangular shape with Mo-ZZ edges. This is another indication of the Mo-rich growth condition discussed above. Our proposed method could reveal that the thermolysis at elevated temperature shows the detailed formation progress of MoS_2 on graphene inside the TEM column.

In addition, Figure 5 shows time-elapsed images of a reconstructed object function during the reknitting progress of a MoS_2 cluster on graphene while holding temperature at 500 °C. In Figure 5a, a sub-nanometer scale hole defect exists between two MoS_2 clusters. The hole defect is observed upon scan, confirming that it is not created by electron-beam irradiation. The hole defect shows Mo-ZZ and S-ZZ edges. Mo adatoms with bright intensity are noted by cyan dashed circles. Then, the hole defects start to reknit with diffusion of atoms and atomic reconstruction (Figure 5b). The images obtained show the MoS_2 cluster, noted by an orange solid line, to be rearranged with roto-translational motion; however, a hole defect exists (Figure 5b). This shows that the roto-translational motion of MoS_2 is possible on graphene as theoretically expected.[40] Also, the atoms and clusters on graphene are highly mobile (Figures S2 and S3). Thermal energy and the electron beam may mobilize the atoms and MoS_x/MoS_2 cluster to overcome the diffusion barrier. As shown in Figure 5c, the MoS_2 cluster finally reknits the hole defect. The MoS_2 cluster has been reknitted and merged with the mirror twin boundary, as denoted by a red dashed box. The mirror twin boundary is along the S-ZZ edge direction and is composed of four-

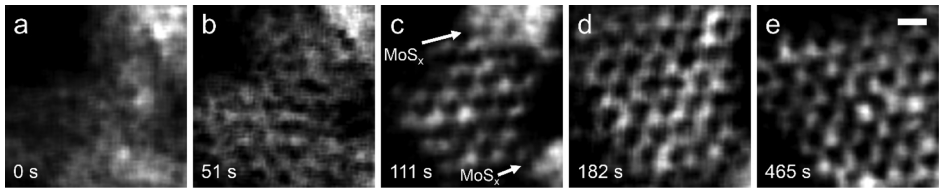

Figure 4. Time-elapsed images of the reconstructed object function showing MoS_2 formation progress on graphene with temperature holding at 500 °C. The elapsed time is shown in the lower left of each image. (a) MoS_x cluster is adsorbed on the graphene substrates. (b) MoS_x reconstructs the MoS_2 cluster. (c) MoS_2 cluster shows a truncated triangular shape with Mo-ZZ, Mo-Klein, and S-ZZ edges. The remaining MoS_x clusters are denoted by white solid arrows. (d) Upside MoS_x cluster transforms into MoS_2. (e) Downside MoS_x clusters also transformed into MoS_2. The MoS_2 cluster shows a triangular shape with Mo-ZZ edges. The scale bar is 0.5 nm.

https://doi.org/10.1021/acsomega.1c03002
ACS Omega 2021, 6, 21623−21630

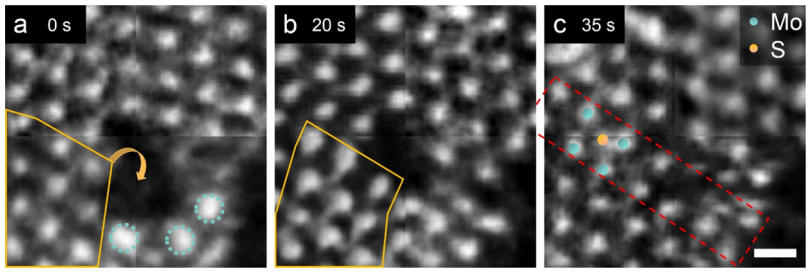

Figure 5. (a−c) Time-elapsed images of the reconstructed object function of MoS_2 reknitting progress on graphene with temperature holding at 500 °C. The elapsed time is shown in the upper left of each image. (a) MoS_2 clusters have a hole with Mo-ZZ and S-ZZ edges. Mo adatoms are noted by cyan dashed circles. (b) Hole starts to reknit with diffusion and atomic reconstruction. The orange solid line in (a,b) shows the roto-translational motion of MoS_2 clusters. (c) Hole has reknitted and shows a mirror twin boundary, as denoted by a red dashed box. Mo and S atoms are represented by cyan and orange spheres, respectively. The scale bar is 0.5 nm..

membered rings. Note that the mirror twin boundary connecting sulfur edges is under a locally Mo-rich condition. Previous studies reported that chalcogen deficiency can affect the formation of mirror twin boundaries. It should be related to our growth condition. Also, among sulfur-deficient twin boundaries, the formation energy of the four-membered-ring twin boundary is the lowest.[41] We demonstrate that the revealed mirror twin boundary formation here originated because of Mo-rich growth conditions and minimization of the total energy of the hole and grain boundary. Recent studies have observed and predicted that the mirror twin boundary is formed by the merging of two grains.[41−43] To the best of our knowledge, this is the first in situ observation of mirror twin boundary formation by coalescence of MoS_2 clusters and their atomic-scale progress. Our method revealed that the reknitting progress during in situ synthesis of MoS_2 involves the removal of atomic defects and roto-translational displacement of clusters with in situ heating STEM experiments.

Because the electronic and optoelectronic properties of MoS_2/graphene stack vary with the twist angle of the layers,[44,45] we analyzed the twist angles using TEM (Figure S4) TEM images of MoS_2 monolayers grown on graphene using the in situ heating holder were taken at room temperature (RT) with an acceleration voltage of 80 kV. FFTs of the TEM images show mixed spot patterns of crystalline MoS_2 and graphene (Figure S4a−e). As shown in the histogram of the observed misorientation angles between MoS_2 and graphene (Figure S4f), MoS_2 clusters are oriented randomly without preferential direction, indicating non-epitaxial growth of MoS_2 on graphene. As observed in Figure 5, the roto-translational displacement of the MoS_2/graphene heterostructure with thermal energy at elevated temperatures occurs and plays a critical role in the reorientation of MoS_2 clusters to be relaxed to a thermodynamically stable orientation.[40,46] Nevertheless, growth conditions such as relatively low temperature and ultrahigh vacuum could result in nonepitaxial growth.[47,48] Also, since we rapidly cooled down the specimen to RT, it may be stuck as the thermal energy decreases before the MoS_2 clusters relax to the corresponding graphene lattice. The effect of trapping of MoS_2 clusters by contaminants or the precursor can also affect the nonepitaxial characteristic of MoS_2 on graphene.[19] Considering that the MoS_2 growth on graphene commonly exhibits van der Waals epitaxial growth,[10,49−51] the nonepitaxial growth of MoS_2 on graphene here would be also useful for twistronics and their applications.

3. CONCLUSIONS

In summary, we performed an in situ STEM study on the formation of MoS_2 on graphene at 500 °C using the DeepSTEM framework. The MoS_2 was synthesized directly on suspended graphene by thermolysis. The DeepSTEM framework successfully reconstructed the object function from HAADF-STEM imaging, which enabled the accurate determination of MoS_2 structures and observation of the dynamics of in situ STEM. In situ STEM studies have been using conventional filtering interpretation methods to interpret atomic-scale behavior. However, these methods have limitations in terms of interpreting electron micrographs deteriorated by an imperfect optic system. Because the object function is the absolute value of the exit wave, the DeepSTEM framework to reconstruct the object function enables in situ STEM observation of atomic-scale behaviors of MoS_2 clusters with correcting the imperfect optic system. The real-time structural formation and evolution from a MoS_x cluster to the triangular MoS_2 cluster were observed. In addition, the reknitting progress of MoS_2 clusters with hole defects was observed. Furthermore, the formation of the mirror twin boundary was revealed during the merging of MoS_2 clusters. Interestingly, note that the MoS_2 clusters show nonepitaxial growth on graphene, as revealed by atomic-resolution TEM. This in situ study provides atomic-scale insights into the formation of MoS_2/graphene heterostructures and the possible use of deep-learning techniques in 2D material research. The combination of in situ STEM experimental images and the deep-learning framework is promising for further exploring novel structures and properties.

4. EXPERIMENTAL SECTION

4.1. Fabrication of Suspended Graphene and Drop Casting of the MoS_2 Precursor. Graphene was synthesized by CVD on 25 μm-thick Cu foil (99.8%, Alfa-Aesar, US). The temperature was increased to 1000 °C under a hydrogen atmosphere (30 sccm) for 40 min, and then, the specimen was maintained for 20 min under a hydrogen atmosphere (30 sccm). After that, methane gas (5 sccm) was added into the chamber and heated for 25 min at 1000 °C. After the growth, the hot zone was opened to cool the specimen to RT. The transfer of the graphene films onto an MEMS-based heating chip was performed by wet etching of the copper substrate after a spin coating of poly(methyl methacrylate). A PMMA solution was spin-coated onto the surface of the as-grown graphene films on Cu foil at a speed of 3000 rpm for 100 s. To ensure the binding of PMMA onto graphene, it was baked at

https://doi.org/10.1021/acsomega.1c03002
ACS Omega 2021, 6, 21623−21630

130 °C for 10 min. Then, the specimen was placed into a solution of sodium persulfate ($Na_2S_2O_8$ with a concentration of 0.2 g in 1 mL of distilled water). After etching the copper substrate and rinsing the PMMA/graphene stack, it was transferred onto a heating chip. To enhance the attachment, this heating chip was heated at 120 °C for 30 min under ambient conditions. It was then soaked in acetone for a day to remove the PMMA. Holes were etched by FIB for the suspended graphene support before the transfer progress. The diameter of the circular holes was 1.2 μm. $(NH_4)_2MoS_4$ was dissolved in DMF with 0.1 wt % solution. The solution was sonicated for 1 h. Then, the solution of 0.5 μL was dropped onto the suspended graphene/heating chip and dried at 120 °C for 30 min under the ambient condition to vaporize the solvent.

4.2. In Situ STEM and MoS_2 Orientation Analysis. In situ STEM was conducted using an aberration-corrected FEI Titan G2 cube 60−300 transmission electron microscope (Thermo Fisher Scientific, US) equipped with probe and image correctors and a monochromator. It was operated at 200 kV. The convergence angle was 26.6 mrad, and a beam current of 85 pA was used to obtain HAADF-STEM images. HAADF detector angles were 50.5−200 mrad, and dwell times of 4−16 μs were used. In situ formation of MoS_2 by thermolysis was conducted using a Wildfire in situ heating holder (DENSsolutions, Netherlands). The heating chip with the MoS_2 precursor on suspended graphene was loaded onto the in situ heating holder. The specimen was heated from RT to 500 °C in ∼1 s in the TEM column, and the elevated temperature was maintained during observation. The orientation between MoS_2 and graphene was analyzed using the microscope with atomic-resolution TEM images.

4.3. Training Data. Atomic-resolution images of MoS_2/Gr prepared by the abovementioned method were obtained from aberration-corrected STEM with an acceleration voltage of 200 kV. The original 700 atomic-resolution STEM images have 1024 × 1024 pixels. Images were cropped into 128 × 128 pixels images, yielding a data set of 44,800 images. Each image has several hundred atoms. Finally, over 4,480,000 samples were used to train the DeepSTEM framework because the same atoms cannot be identified. The architecture of the DeepSTEM framework is shown in Table S1.

■ ASSOCIATED CONTENT

Supporting Information

The Supporting Information is available free of charge at https://pubs.acs.org/doi/10.1021/acsomega.1c03002.

Fabrication of suspended graphene and drop casting of the MoS_2 precursor, in situ STEM and MoS_2 orientation analysis, training data, images of the in situ heating holder and chip with suspended graphene, time-elapsed HAADF-STEM images of mobile Mo atoms on graphene at 500 °C, time-elapsed HAADF-STEM images of the roto-translational motion of MoS_2 on graphene at 500 °C, atomic-resolution TEM image of MoS_2 clusters on graphene and histogram of misorientation angles, HAADF-STEM image of MoS_2 clusters, architecture of the DeepSTEM framework and Appendix A: autoencoder (PDF)

■ AUTHOR INFORMATION

Corresponding Author

Zonghoon Lee − *Center for Multidimensional Carbon Materials, Institute for Basic Science (IBS), Ulsan 44919, Republic of Korea; Department of Materials Science and Engineering, Ulsan National Institute of Science and Technology (UNIST), Ulsan 44919, Republic of Korea;* orcid.org/0000-0003-3246-4072; Email: zhlee@unist.ac.kr

Authors

Yeongdong Lee − *Center for Multidimensional Carbon Materials, Institute for Basic Science (IBS), Ulsan 44919, Republic of Korea; Department of Materials Science and Engineering, Ulsan National Institute of Science and Technology (UNIST), Ulsan 44919, Republic of Korea;* orcid.org/0000-0001-9749-5270

Jongyeong Lee − *Center for Multidimensional Carbon Materials, Institute for Basic Science (IBS), Ulsan 44919, Republic of Korea; Department of Materials Science and Engineering, Ulsan National Institute of Science and Technology (UNIST), Ulsan 44919, Republic of Korea;* orcid.org/0000-0002-3456-0300

Handolsam Chung − *Center for Multidimensional Carbon Materials, Institute for Basic Science (IBS), Ulsan 44919, Republic of Korea; Department of Materials Science and Engineering, Ulsan National Institute of Science and Technology (UNIST), Ulsan 44919, Republic of Korea*

Jaemin Kim − *Center for Multidimensional Carbon Materials, Institute for Basic Science (IBS), Ulsan 44919, Republic of Korea; Department of Materials Science and Engineering, Ulsan National Institute of Science and Technology (UNIST), Ulsan 44919, Republic of Korea;* orcid.org/0000-0001-8675-7271

Complete contact information is available at: https://pubs.acs.org/10.1021/acsomega.1c03002

Author Contributions

Y.L. and J.L. contributed equally to this work. The manuscript was written through contributions of all authors. All authors have given approval to the final version of the manuscript.

Notes

The authors declare no competing financial interest.

■ ACKNOWLEDGMENTS

This work was supported by the Institute for Basic Science (IBS-R019-D1).

■ REFERENCES

(1) Khan, K.; Tareen, A. K.; Aslam, M.; Wang, R.; Zhang, Y.; Mahmood, A.; Ouyang, Z.; Zhang, H.; Guo, Z. Recent developments in emerging two-dimensional materials and their applications. *J. Mater. Chem. C* **2020**, *8*, 387−440.

(2) Hong, S.; Lee, C.-S.; Lee, M.-H.; Lee, Y.; Ma, K. Y.; Kim, G.; Yoon, S. I.; Ihm, K.; Kim, K.-J.; Shin, T. J.; Kim, S. W.; Jeon, E.-c.; Jeon, H.; Kim, J.-Y.; Lee, H.-I.; Lee, Z.; Antidormi, A.; Roche, S.; Chhowalla, M.; Shin, H.-J.; Shin, H. S. Ultralow-dielectric-constant amorphous boron nitride. *Nature* **2020**, *582*, 511−514.

(3) Lee, C.-S.; Shin, K. W.; Song, H.-J.; Park, H.; Cho, Y.; Im, D.-H.; Lee, H.; Lee, J.-H.; Won, J. Y.; Chung, J. G.; Kim, C.; Byun, K.-E.; Lee, E.-K.; Kim, Y.; Ko, W.; Lim, H. J.; Park, S.; Shin, H.-J. Fabrication of Metal/Graphene Hybrid Interconnects by Direct

Graphene Growth and Their Integration Properties. *Adv. Electron. Mater.* **2018**, *4*, 1700624.
(4) Lo, C.-L.; Helfrecht, B. A.; He, Y.; Guzman, D. M.; Onofrio, N.; Zhang, S.; Weinstein, D.; Strachan, A.; Chen, Z. Opportunities and challenges of 2D materials in back-end-of-line interconnect scaling. *J. Appl. Phys.* **2020**, *128*, 080903.
(5) Novoselov, K. S.; Mishchenko, A.; Carvalho, A.; Castro Neto, A. H. 2D materials and van der Waals heterostructures. *Science* **2016**, *353*, aac9439.
(6) Manzeli, S.; Ovchinnikov, D.; Pasquier, D.; Yazyev, O. V.; Kis, A. 2D transition metal dichalcogenides. *Nat. Rev. Mater.* **2017**, *2*, 17033.
(7) Novoselov, K. S.; Jiang, D.; Schedin, F.; Booth, T. J.; Khotkevich, V. V.; Morozov, S. V.; Geim, A. K. Two-dimensional atomic crystals. *Proc. Natl. Acad. Sci. U.S.A.* **2005**, *102*, 10451−10453.
(8) Kaushik, N.; Nipane, A.; Basheer, F.; Dubey, S.; Grover, S.; Deshmukh, M. M.; Lodha, S. Schottky barrier heights for Au and Pd contacts to MoS_2. *Appl. Phys. Lett.* **2014**, *105*, 113505.
(9) Liu, Y.; Wu, H.; Cheng, H.-C.; Yang, S.; Zhu, E.; He, Q.; Ding, M.; Li, D.; Guo, J.; Weiss, N. O.; Huang, Y.; Duan, X. Toward barrier free contact to molybdenum disulfide using graphene electrodes. *Nano Lett.* **2015**, *15*, 3030−3034.
(10) Shi, Y.; Zhou, W.; Lu, A.-Y.; Fang, W.; Lee, Y.-H.; Hsu, A. L.; Kim, S. M.; Kim, K. K.; Yang, H. Y.; Li, L.-J.; Idrobo, J.-C.; Kong, J. van der Waals Epitaxy of MoS_2 Layers Using Graphene As Growth Templates. *Nano Lett.* **2012**, *12*, 2784−2791.
(11) Wang, H. W.; Skeldon, P.; Thompson, G. E.; Wood, G. C. Synthesis and characterization of molybdenum disulphide formed from ammonium tetrathiomolybdate. *J. Mater. Sci.* **1997**, *32*, 497−502.
(12) Sygellou, L. An in-situ photoelectron spectroscopy study of the thermal processing of ammonium tetrathiomolybdate, $(NH_4)_2MoS_4$, precursor. *Appl. Surf. Sci.* **2019**, *476*, 1079−1085.
(13) Yang, J.; Gu, Y.; Lee, E.; Lee, H.; Park, S. H.; Cho, M.-H.; Kim, Y. H.; Kim, Y.-H.; Kim, H. Wafer-scale synthesis of thickness-controllable MoS_2 films via solution-processing using a dimethylformamide/n-butylamine/2-aminoethanol solvent system. *Nanoscale* **2015**, *7*, 9311−9319.
(14) Yang, H.; Giri, A.; Moon, S.; Shin, S.; Myoung, J.-M.; Jeong, U. Highly scalable synthesis of MoS_2 thin films with precise thickness control via polymer-assisted deposition. *Chem. Mater.* **2017**, *29*, 5772−5776.
(15) Zhu, Y.; Yuan, D.; Zhang, H.; Xu, T.; Sun, L. Atomic-scale insights into the formation of 2D crystals from in situ transmission electron microscopy. *Nano Res.* **2021**, *14*, 1650−1658.
(16) Mishra, R.; Ishikawa, R.; Lupini, A. R.; Pennycook, S. J. Single-atom dynamics in scanning transmission electron microscopy. *MRS Bull.* **2017**, *42*, 644−652.
(17) Su, C.; Tripathi, M.; Yan, Q.-B.; Wang, Z.; Zhang, Z.; Hofer, C.; Wang, H.; Basile, L.; Su, G.; Dong, M.; Meyer, J. C.; Kotakoski, J.; Kong, J.; Idrobo, J.-C.; Susi, T.; Li, J. Engineering single-atom dynamics with electron irradiation. *Sci. Adv.* **2019**, *5*, No. eaav2252.
(18) Fei, L.; Lei, S.; Zhang, W.-B.; Lu, W.; Lin, Z.; Lam, C. H.; Chai, Y.; Wang, Y. Direct TEM observations of growth mechanisms of two-dimensional MoS_2 flakes. *Nat. Commun.* **2016**, *7*, 12206.
(19) Sang, X.; Li, X.; Puretzky, A. A.; Geohegan, D. B.; Xiao, K.; Unocic, R. R. Atomic Insight into Thermolysis-Driven Growth of 2D MoS_2. *Adv. Funct. Mater.* **2019**, *29*, 1902149.
(20) Kondekar, N.; Boebinger, M. G.; Tian, M.; Kirmani, M. H.; McDowell, M. T. The Effect of Nickel on MoS_2 Growth Revealed with in Situ Transmission Electron Microscopy. *ACS Nano* **2019**, *13*, 7117−7126.
(21) Morgan, A. J.; Martin, A. V.; D'Alfonso, A. J.; Putkunz, C. T.; Allen, L. J. Direct exit-wave reconstruction from a single defocused image. *Ultramicroscopy* **2011**, *111*, 1455−1460.
(22) Kirkland, E. J. Improved high resolution image processing of bright field electron micrographs: I. Theory. *Ultramicroscopy* **1984**, *15*, 151−172.
(23) Nellist, P. D.; Pennycook, S. J. Accurate structure determination from image reconstruction in ADF STEM. *J. Microsc.* **1998**, *190*, 159−170.
(24) Nellist, P. D.; Pennycook, S. J. Probe and object function reconstruction in incoherent scanning transmission electron microscope imaging. *Scanning Microsc.* **1997**, *11*, 81−90.
(25) Kazubek, M. Wavelet domain image denoising by thresholding and Wiener filtering. *IEEE Signal Process. Lett.* **2003**, *10*, 324−326.
(26) Ede, J. M. Deep learning in electron microscopy. *Mach. Learn.: Sci. Technol.* **2021**, *2*, 011004.
(27) Madsen, J.; Liu, P.; Kling, J.; Wagner, J. B.; Hansen, T. W.; Winther, O.; Schiøtz, J. A Deep Learning Approach to Identify Local Structures in Atomic-Resolution Transmission Electron Microscopy Images. *Adv. Theory Simul.* **2018**, *1*, 1800037.
(28) Lee, J.; Lee, Y.; Kim, J.; Lee, Z. Contrast Transfer Function-Based Exit-Wave Reconstruction and Denoising of Atomic-Resolution Transmission Electron Microscopy Images of Graphene and Cu Single Atom Substitutions by Deep Learning Framework. *Nanomaterials* **2020**, *10*, 1977.
(29) Nellist, P. D.; Pennycook, S. J. The principles and interpretation of annular dark-field Z-contrast imaging. *Adv. Imaging Electron Phys.* **2000**, *113*, 147−203.
(30) Kramer, M. A. Nonlinear Principal Component Analysis Using Autoassociative Neural Networks. *AIChE J.* **1991**, *37*, 233−243.
(31) Zemlin, F.; Weiss, K.; Schiske, P.; Kunath, W.; Herrmann, K.-H. Coma-free alignment of high resolution electron microscopes with the aid of optical diffractograms. *Ultramicroscopy* **1978**, *3*, 49−60.
(32) Kingma, D. P.; Ba, J. Adam: A Method for Stochastic Optimization. arXiv.org, e-Print Arch., Comput. Sci.. **2014**, arXiv:1412.6980.
(33) Geim, A. K.; Novoselov, K. S. The rise of graphene. *Nat. Mater.* **2007**, *6*, 183−191.
(34) Li, X.; Cai, W.; An, J.; Kim, S.; Nah, J.; Yang, D.; Piner, R.; Velamakanni, A.; Jung, I.; Tutuc, E.; Banerjee, S. K.; Colombo, L.; Ruoff, R. S. Large-Area Synthesis of High-Quality and Uniform Graphene Films on Copper Foils. *Science* **2009**, *324*, 1312−1314.
(35) van der Zande, A. M.; Huang, P. Y.; Chenet, D. A.; Berkelbach, T. C.; You, Y.; Lee, G.-H.; Heinz, T. F.; Reichman, D. R.; Muller, D. A.; Hone, J. C. Grains and grain boundaries in highly crystalline monolayer molybdenum disulphide. *Nat. Mater.* **2013**, *12*, 554−561.
(36) Xu, W.; Li, S.; Zhou, S.; Lee, J. K.; Wang, S.; Sarwat, S. G.; Wang, X.; Bhaskaran, H.; Pasta, M.; Warner, J. H. Large dendritic monolayer MoS_2 grown by atmospheric pressure chemical vapor deposition for electrocatalysis. *ACS Appl. Mater. Interfaces* **2018**, *10*, 4630−4639.
(37) Schweiger, H.; Raybaud, P.; Kresse, G.; Toulhoat, H. Shape and edge sites modifications of MoS_2 catalytic nanoparticles induced by working conditions: A theoretical study. *J. Catal.* **2002**, *207*, 76−87.
(38) Zhu, D.; Shu, H.; Jiang, F.; Lv, D.; Asokan, V.; Omar, O.; Yuan, J.; Zhang, Z.; Jin, C. Capture the growth kinetics of CVD growth of two-dimensional MoS_2. *npj 2D Mater. Appl.* **2017**, *1*, 8.
(39) Pan, H.; Zhang, Y.-W. Edge-dependent structural, electronic and magnetic properties of MoS_2 nanoribbons. *J. Mater. Chem.* **2012**, *22*, 7280−7290.
(40) Wang, L.; Zhou, X.; Ma, T.; Liu, D.; Gao, L.; Li, X.; Zhang, J.; Hu, Y.; Wang, H.; Dai, Y.; Luo, J. Superlubricity of a graphene/MoS_2 heterostructure: a combined experimental and DFT study. *Nanoscale* **2017**, *9*, 10846−10853.
(41) Batzill, M. Mirror twin grain boundaries in molybdenum dichalcogenides. *J. Phys.: Condens. Matter* **2018**, *30*, 493001.
(42) Kim, J. H.; Kim, S. Y.; Park, S. O.; Jung, G. Y.; Song, S.; Sohn, A.; Kim, S. W.; Kwak, S. K.; Kwon, S. Y.; Lee, Z. Antiphase Boundaries as Faceted Metallic Wires in 2D Transition Metal Dichalcogenides. *Adv. Sci.* **2020**, *7*, 2000788.
(43) Zhou, S.; Wang, S.; Shi, Z.; Sawada, H.; Kirkland, A. I.; Li, J.; Warner, J. H. Atomically sharp interlayer stacking shifts at anti-phase grain boundaries in overlapping MoS_2 secondary layers. *Nanoscale* **2018**, *10*, 16692−16702.

https://doi.org/10.1021/acsomega.1c03002
ACS Omega 2021, 6, 21623−21630

(44) Du, L.; Yu, H.; Liao, M.; Wang, S.; Xie, L.; Lu, X.; Zhu, J.; Li, N.; Shen, C.; Chen, P.; Yang, R.; Shi, D.; Zhang, G. Modulating PL and electronic structures of MoS_2/graphene heterostructures via interlayer twisting angle. *Appl. Phys. Lett.* **2017**, *111*, 263106.
(45) Liao, M.; Wu, Z.-W.; Du, L.; Zhang, T.; Wei, Z.; Zhu, J.; Yu, H.; Tang, J.; Gu, L.; Xing, Y.; Yang, R.; Shi, D.; Yao, Y.; Zhang, G. Twist angle-dependent conductivities across MoS_2/graphene heterojunctions. *Nat. Commun.* **2018**, *9*, 4068.
(46) Büch, H.; Rossi, A.; Forti, S.; Convertino, D.; Tozzini, V.; Coletti, C. Superlubricity of epitaxial monolayer WS_2 on graphene. *Nano Res.* **2018**, *11*, 5946−5956.
(47) Azizi, A.; Eichfeld, S.; Geschwind, G.; Zhang, K.; Jiang, B.; Mukherjee, D.; Hossain, L.; Piasecki, A. F.; Kabius, B.; Robinson, J. A.; Alem, N. Freestanding van der Waals Heterostructures of Graphene and Transition Metal Dichalcogenides. *ACS Nano* **2015**, *9*, 4882−4890.
(48) Shi, J.; Liu, M.; Wen, J.; Ren, X.; Zhou, X.; Ji, Q.; Ma, D.; Zhang, Y.; Jin, C.; Chen, H.; Deng, S.; Xu, N.; Liu, Z.; Zhang, Y. All Chemical Vapor Deposition Synthesis and Intrinsic Bandgap Observation of MoS_2/Graphene Heterostructures. *Adv. Mater.* **2015**, *27*, 7086−7092.
(49) Miwa, J. A.; Dendzik, M.; Grønborg, S. S.; Bianchi, M.; Lauritsen, J. V.; Hofmann, P.; Ulstrup, S. Van der Waals Epitaxy of Two-Dimensional MoS_2−Graphene Heterostructures in Ultrahigh Vacuum. *ACS Nano* **2015**, *9*, 6502−6510.
(50) Ago, H.; Endo, H.; Solís-Fernández, P.; Takizawa, R.; Ohta, Y.; Fujita, Y.; Yamamoto, K.; Tsuji, M. Controlled van der Waals Epitaxy of Monolayer MoS_2 Triangular Domains on Graphene. *ACS Appl. Mater. Interfaces* **2015**, *7*, 5265−5273.
(51) Liu, X.; Balla, I.; Bergeron, H.; Campbell, G. P.; Bedzyk, M. J.; Hersam, M. C. Rotationally Commensurate Growth of MoS_2 on Epitaxial Graphene. *ACS Nano* **2016**, *10*, 1067−1075.

https://doi.org/10.1021/acsomega.1c03002
ACS Omega 2021, 6, 21623−21630